SUPPLEMENTARY INFORMATION FOR

Liquid-liquid Transition and Ice Crystallization in a Machine-Learned Coarse-Grained Water Model

Debdas Dhabal,[a] Rajat Kumar,[a] and Valeria Molinero[a,*]

[a]*Department of Chemistry, University of Utah, Salt Lake City, UT-84112-0850, USA.*

[*]Corresponding author email: valeria.molinero@utah.edu

A. Density correlations in vitrified ML-BOP

To calculate the long-range structural correlations of liquid and glass ML-BOP at different pressures in quenching simulations with 10 K ns^{-1} cooling rate from 298 K to 78 K, we use periodic cubic simulation cells with 8000 ML-BOP water molecules, previously equilibrated for 42 ns at 298 K and the selected pressure. Starting from equilibrated liquid configurations at different pressures, we perform 2 ns simulations to generate 10 independent restart files. These restart files with different initial configurations and velocities are then used for cooling simulations.

To compute $S(0)$ at each state point, we first calculate the water-water structure factor using the following relation(1-3)

$$\boldsymbol{S(\mathbf{q}) = 1 + \frac{1}{N}\langle \sum_{i}^{N}\sum_{j\neq i}^{N} \exp\left(i\mathbf{q}\cdot(\mathbf{r_i}-\mathbf{r_j})\right)\rangle}, \qquad (1)$$

where N is the number of water beads in the simulation box and $\mathbf{r_i}$ is the position vector of atom i. Wave vectors q can be written as, $\mathbf{q} = (\mathbf{n_x}, \mathbf{n_y}, \mathbf{n_z})\mathbf{2\pi/L}$, with L being the length of the simulation box and $\mathbf{n_\alpha}$ are all possible integer values in the three cartesian directions. Wavenumber $\boldsymbol{q = |q|}$ for an isotropic and homogeneous system. We then extrapolate $S(q)$ to $\boldsymbol{q \to 0}$ limit by fitting it with a quadratic equation $\mathbf{f1}(\boldsymbol{q}) = \mathbf{a}\boldsymbol{q}^2 + \mathbf{b}\boldsymbol{q} + \mathbf{c}$ over the range $\mathbf{0.2}$ Å$^{-1} \geq \mathbf{q} \leq \mathbf{1.2}$ Å^{-1}. We also consider quadratic function $\mathbf{f2}(\boldsymbol{q}) = \mathbf{a}\boldsymbol{q}^2 + \mathbf{c}$ (Figures S1 and S2) proposed by Gartner et al.(4) To verify which fitting function results in correct $S(0)$ values for ML-BOP fluids, we calculate the zero-wavenumber structure factor from the isothermal compressibility($\boldsymbol{\kappa_T}$) and density ($\boldsymbol{\rho}$) of liquid at different temperatures from equilibrium simulations at 0.1, 100, and 200 MPa pressures. The $S(0)$ is related to the compressibility as:(5)

$$\boldsymbol{S(0) = \rho k_B T \kappa_T} \qquad (2)$$

where k_B and T are Boltzmann's constant and simulation temperature respectively. Figure S2 indicates that the fitting function $\mathbf{f1}(\boldsymbol{q}) = \mathbf{a}\boldsymbol{q}^2 + \mathbf{b}\boldsymbol{q} + \mathbf{c}$ gives a better estimation of $S(0)$ from our data than $\mathbf{f2}(\boldsymbol{q}) = \mathbf{a}\boldsymbol{q}^2 + \mathbf{c}$. We use the former.

We calculate isothermal compressibility $\boldsymbol{\kappa_T}$ at 0.1, 100 and 200 MPa pressure. The range of temperatures at each pressure varies (see Figure S2). $\boldsymbol{\kappa_T}$ is calculated from the volume fluctuations in a long equilibrium simulation under NpT condition as(6)

$$\boldsymbol{\kappa_T = \frac{1}{\langle V\rangle k_B T}(\langle V^2\rangle - \langle V\rangle^2)}, \qquad (3)$$

Where, V, T and k_B are the box volume, simulation temperature and Boltzmann's constant respectively. We ensure good statistics in the volume fluctuations by performing 500 ns long production simulations at all temperatures and pressures studied. The volume data is saved every 5 ps. Total simulation length is divided into 5 blocks; the $\boldsymbol{\kappa_T}$ value used in the $S(0)$ calculation (see Eq. 2) is the average over all these 5 blocks.

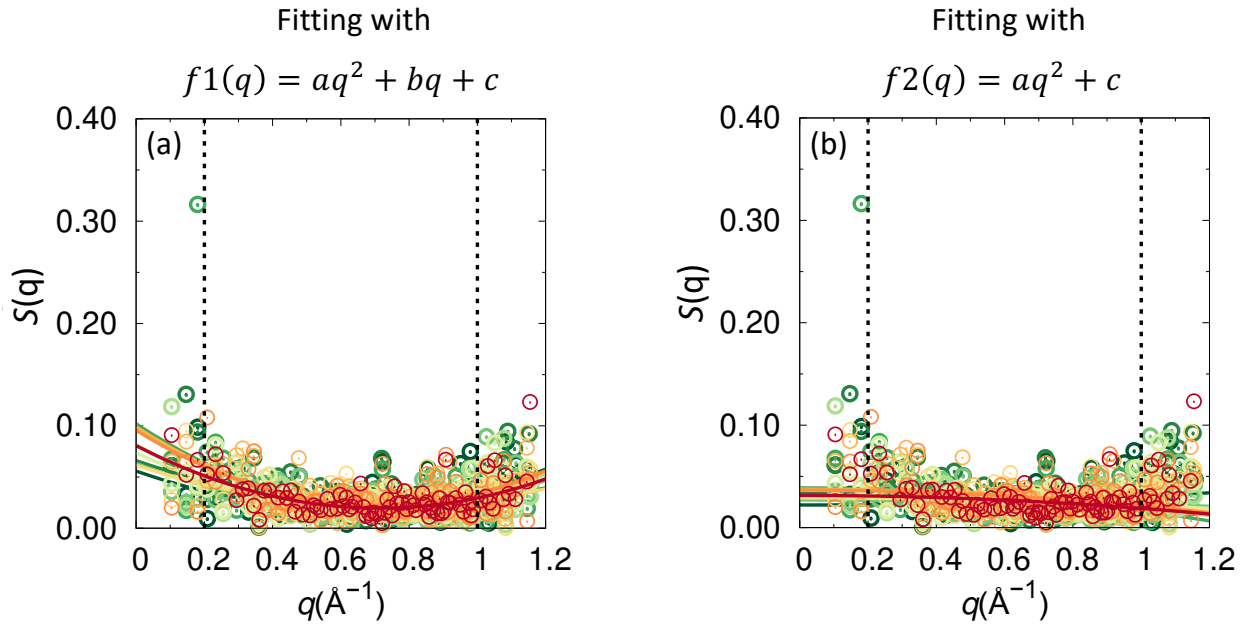

Figure S1. Illustration of the fitting S(q) from 10 independent configurations at 300 MPa and 78 K with two quadratic functions. These configurations were obtained from cooling simulations of 8000 ML-BOP water molecules at 10 K ns^{-1}. $S(q)$ was fitted for q = 0.2 to q = 1 Å^{-1}. The fitting function f1(q)=aq^2+bq+c reproduces best the increase in S(q) at $q \rightarrow 0$ limit and the independently computed isothermal compressibilities, as seen in Figure S2.

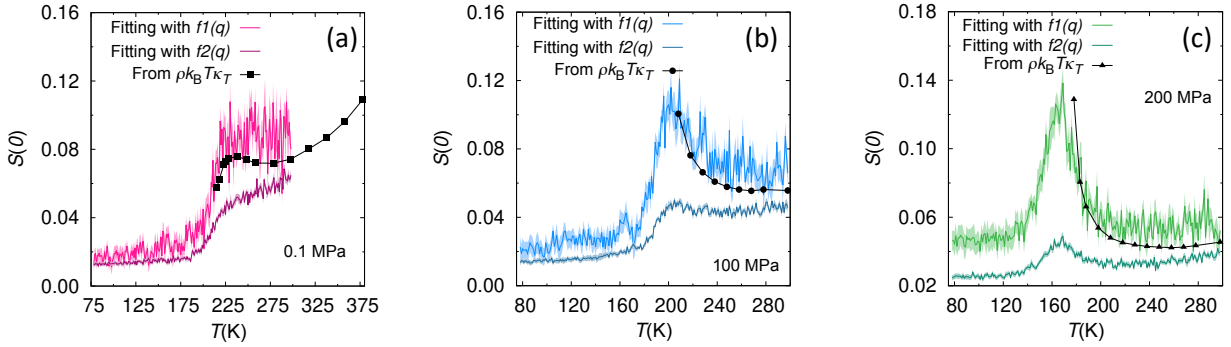

Figure S2. Comparison of $S(0) = \rho k_B T \kappa_T$ with the $S(0)$ obtained from the extrapolation of low wavelength $S(q)$ with two different quadratic fitting functions. Fitting with quadratic function f1(q) reproduces the increase in S(q) at $q \rightarrow 0$ limit, while fitting with f2(q) does not.

B. Determination of the liquid-liquid transition of ML-BOP through phase oscillations

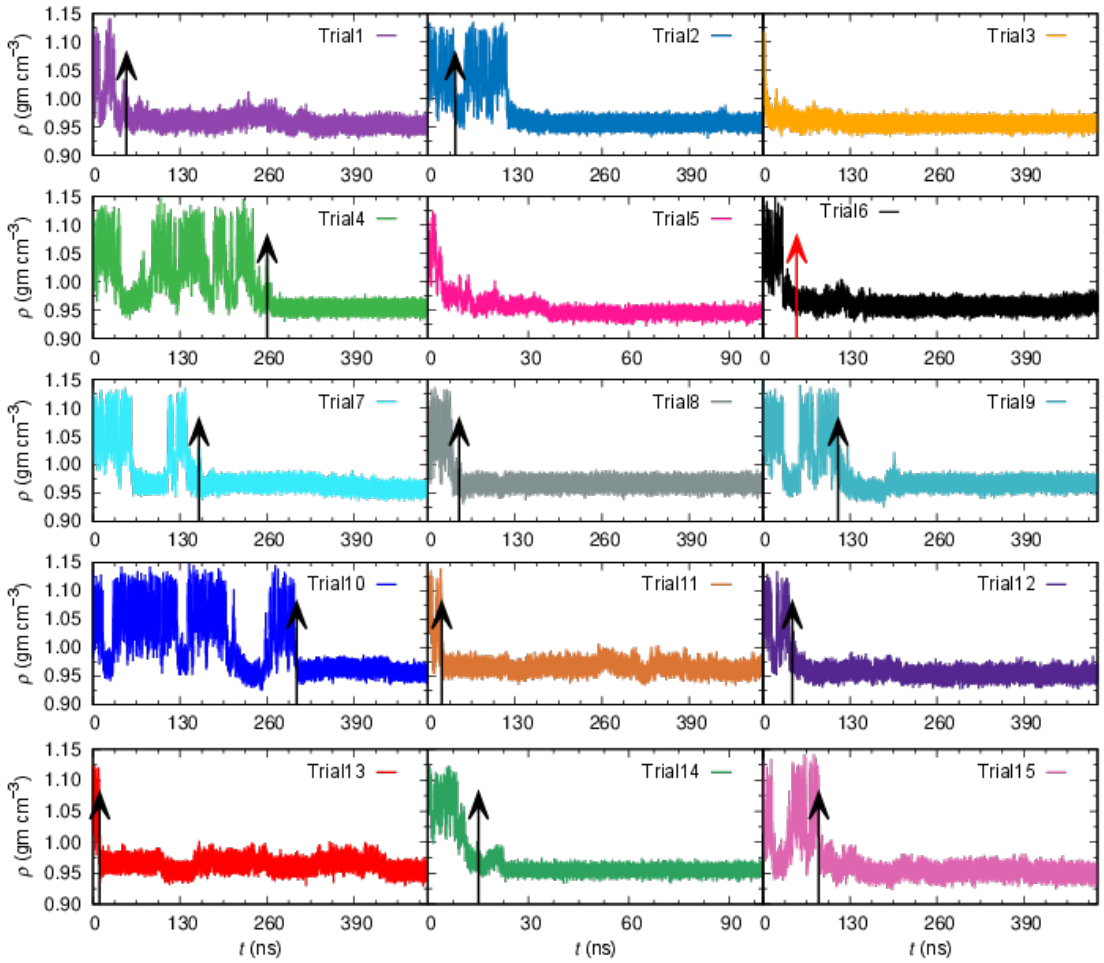

Figure S3. Density as a function of simulation time for 15 individual trial simulations for 192 water molecules systems at 200 MPa and 173 K. The point of crystallization is denoted with an arrow in each plot. System wide density oscillations between LDL and HDL are observed for tens to hundreds of nanoseconds before crystallization.

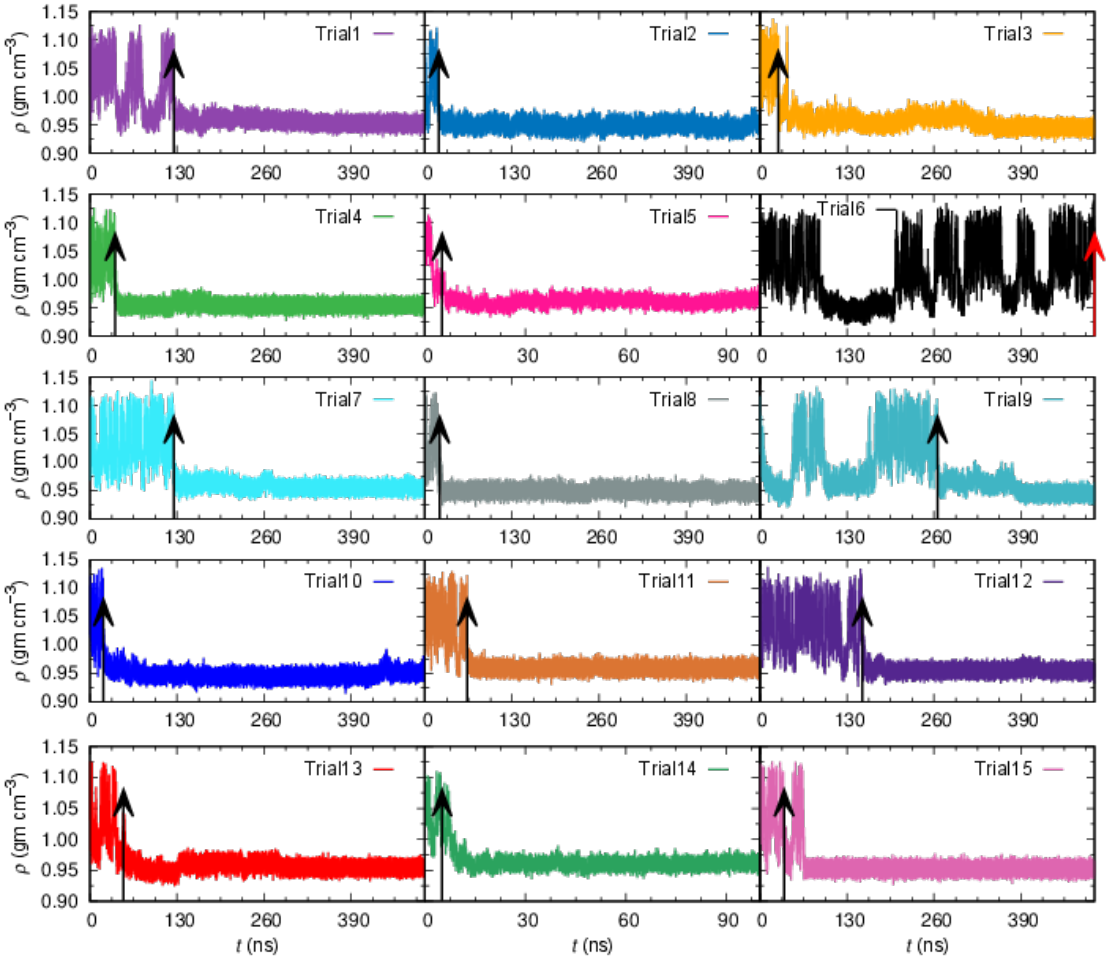

Figure S4. Density as a function of simulation time for 15 individual trial simulations for 192 water molecules systems at 180 MPa and 189 K. The point of crystallization is denoted with an arrow in each plot. System wide density oscillations between LDL and HDL are observed for tens to hundreds of nanoseconds before crystallization.

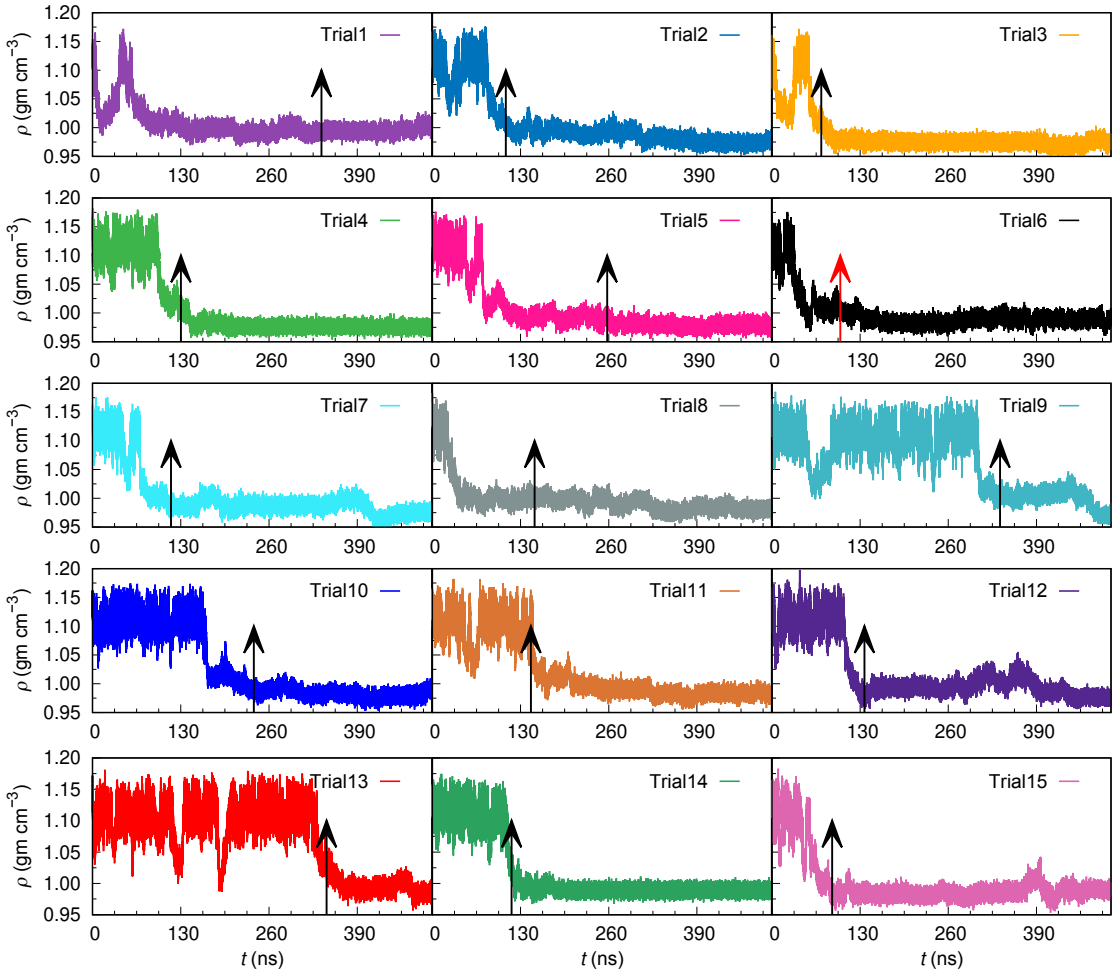

Figure S5. Density as a function of simulation time for 15 individual trial simulations for 192 water molecules systems at 300 MPa and 139 K. The point of crystallization is denoted with an arrow in each plot.

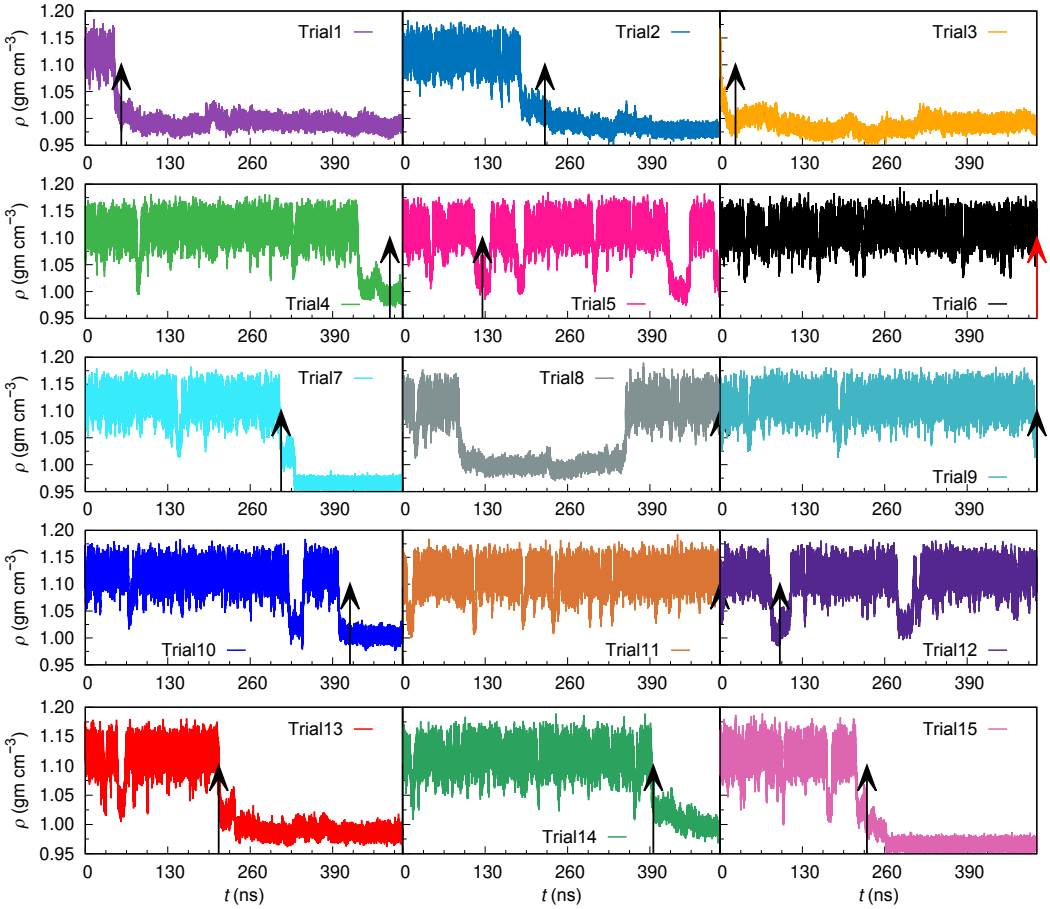

Figure S6. Density as a function of simulation time for 15 individual trial simulations for 192 water molecules systems at 300 MPa and 142 K. The point of crystallization is denoted with an arrow in each plot.

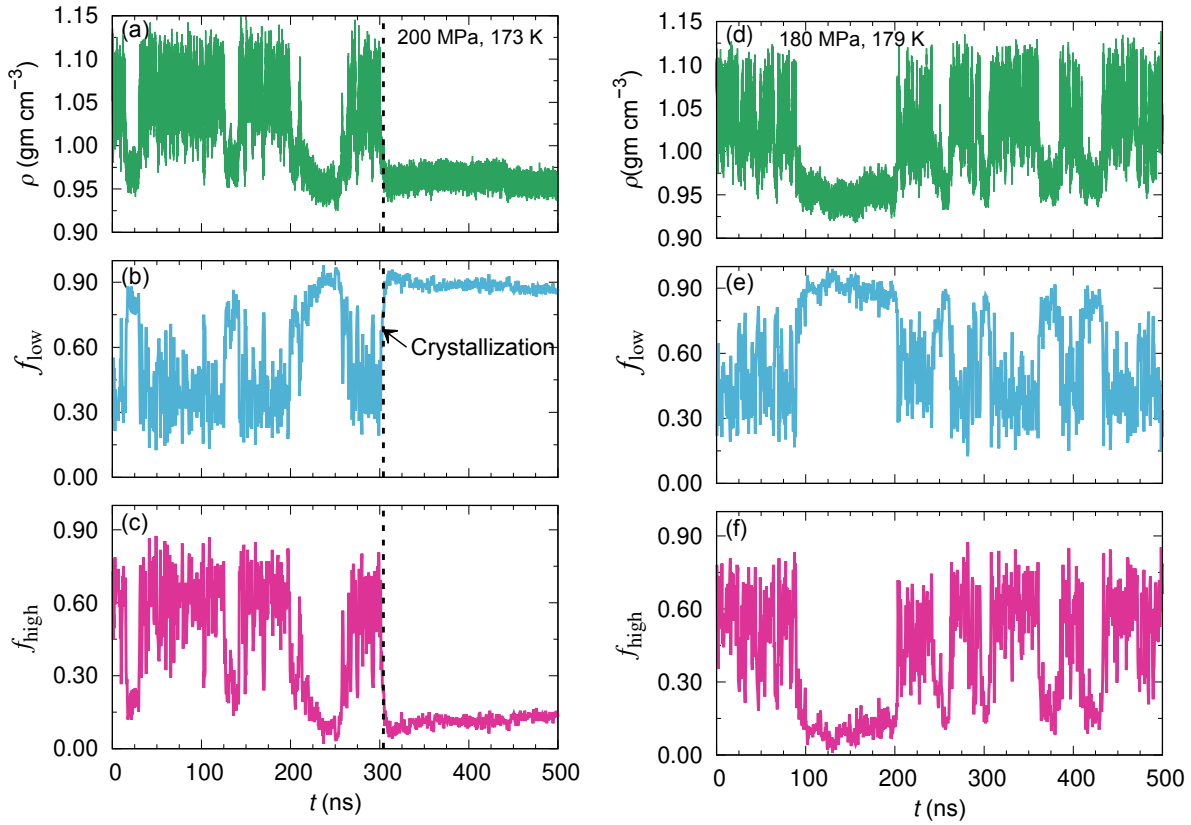

Figure S7. Correlation of density with the fraction of four-coordinated and five-coordinated water molecules during the liquid-liquid transformation of water. f_{high} denotes the fraction of water molecules with coordination five and higher, while f_{low} denotes those with coordination four and lower. Fluctuations in the density of the system directly correlate with fluctuations in f_{low} (or f_{high}).

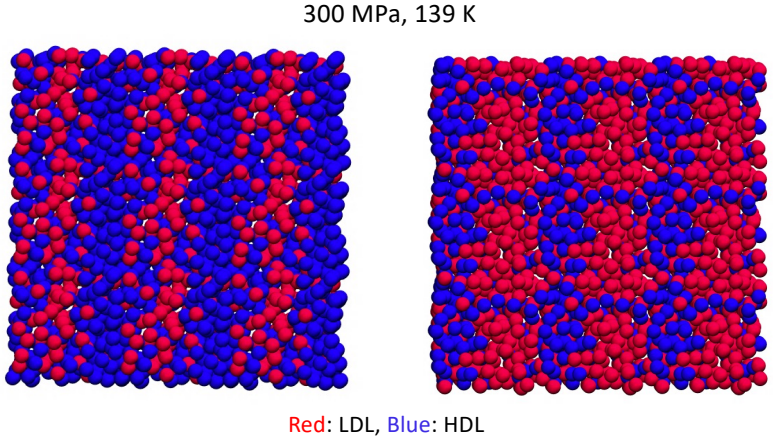

Figure S8. Visualization of the HDL-LDL interface near the barrier region at 300 MPa and 139 K. Low density liquid (LDL) is characterized by local coordination number less than or equal to 4 and high-density liquid (HDL) is characterized by water molecules having local coordination number greater than 4. The figures show a the simulation box with 192 molecules replicated 3 times in each direction, for clarity. The simulation snapshots are prepared using Visual Molecular Dynamics software VMD.[7]

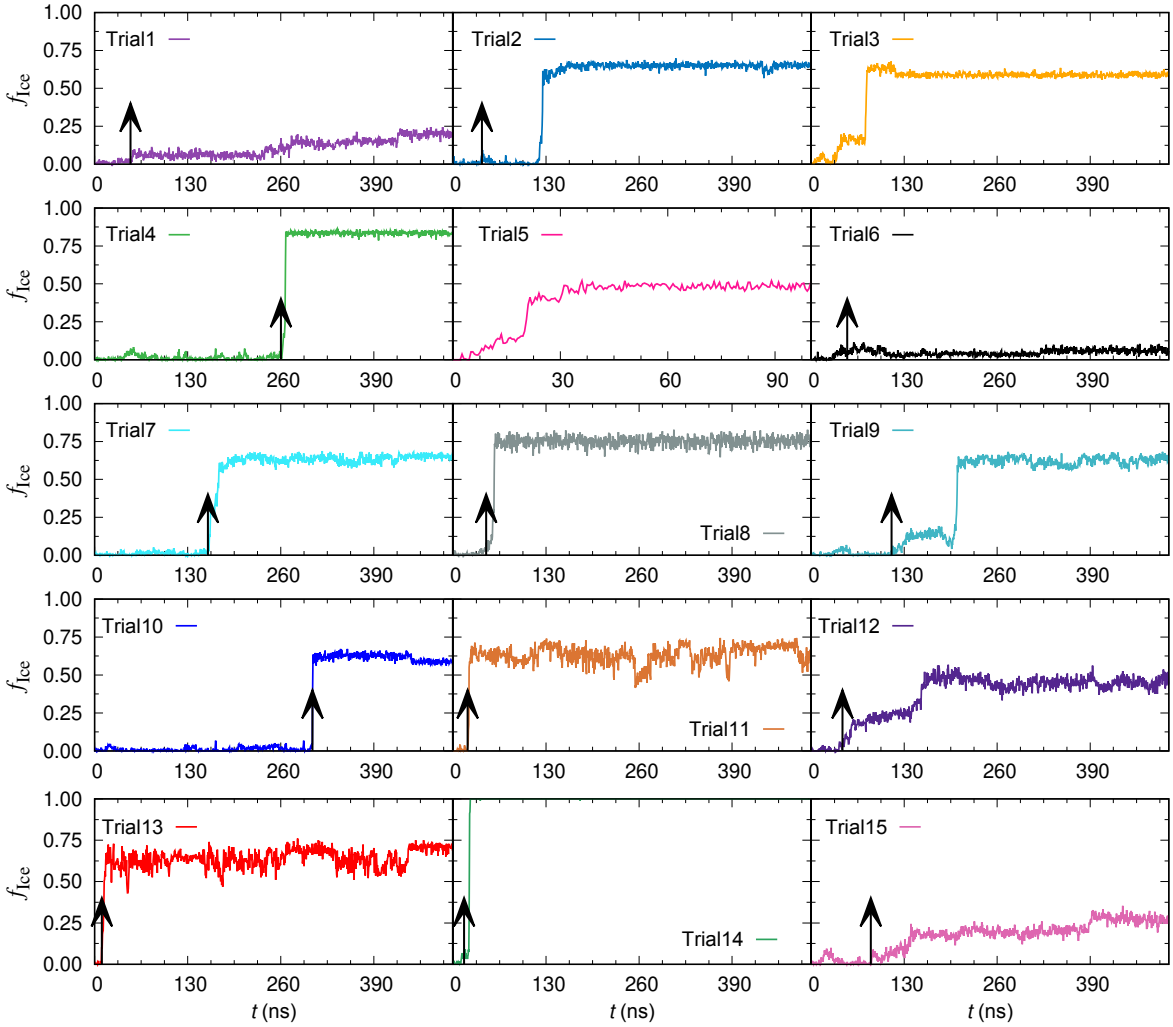

Figure S9. Fractions of cubic and hexagonal ice as a function of simulation time for 15 individual trial simulations for 192 water molecule systems at 200 MPa and 173 K. The point of crystallization using a 6% cutoff is denoted with an arrow in each curve. Only the data before crystallization is used to build histograms of density and energy, from which we compute the relative free energies.

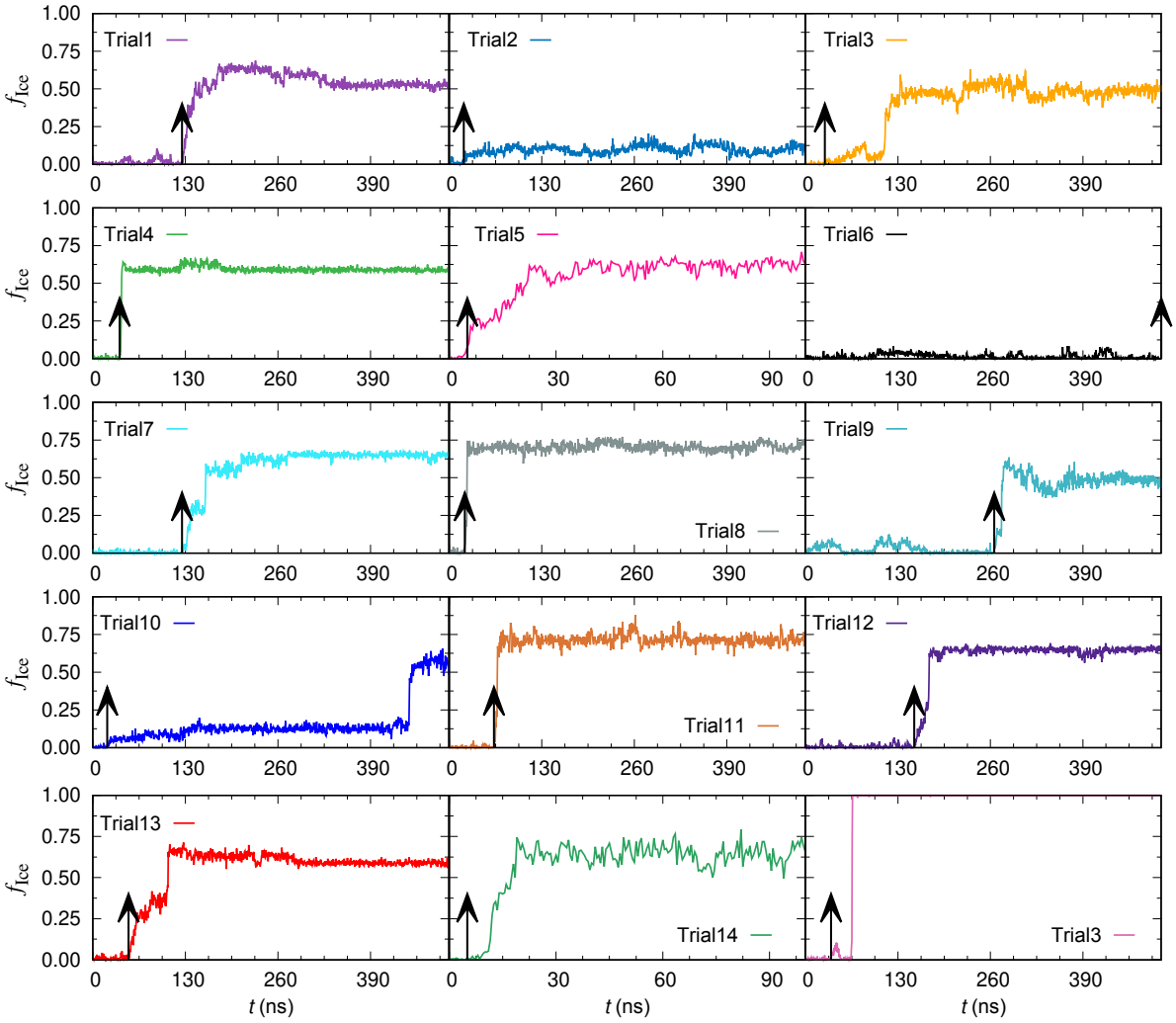

Figure 10. Fractions of cubic and hexagonal ice as a function of simulations time for 15 individual trial simulations at 180 MPa and 179 K. The point of crystallization using a 6% cutoff is denoted with an arrow in each curve.

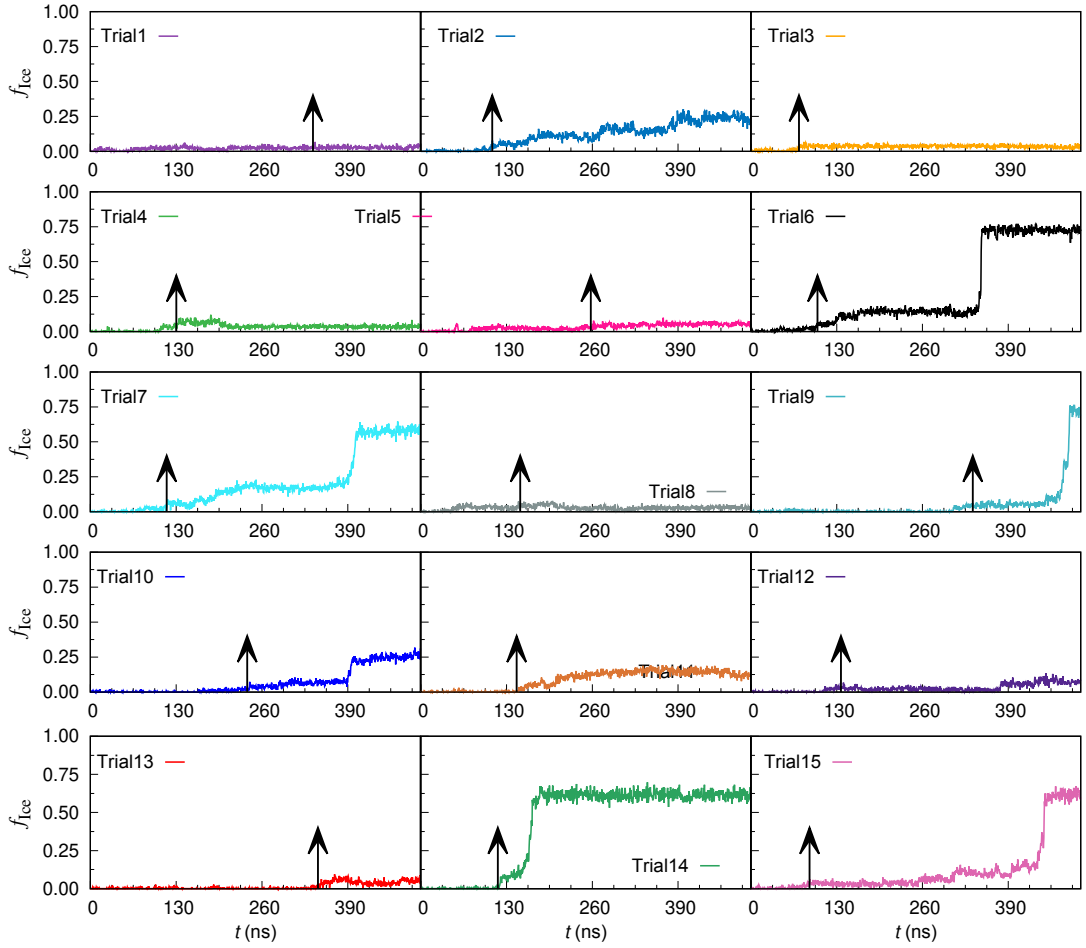

Figure 11. Fractions of cubic and hexagonal ice as a function of simulations time for 15 individual trial simulations at 300 MPa and 139 K. The point of crystallization using a 6% cutoff is denoted with an arrow in each curve.

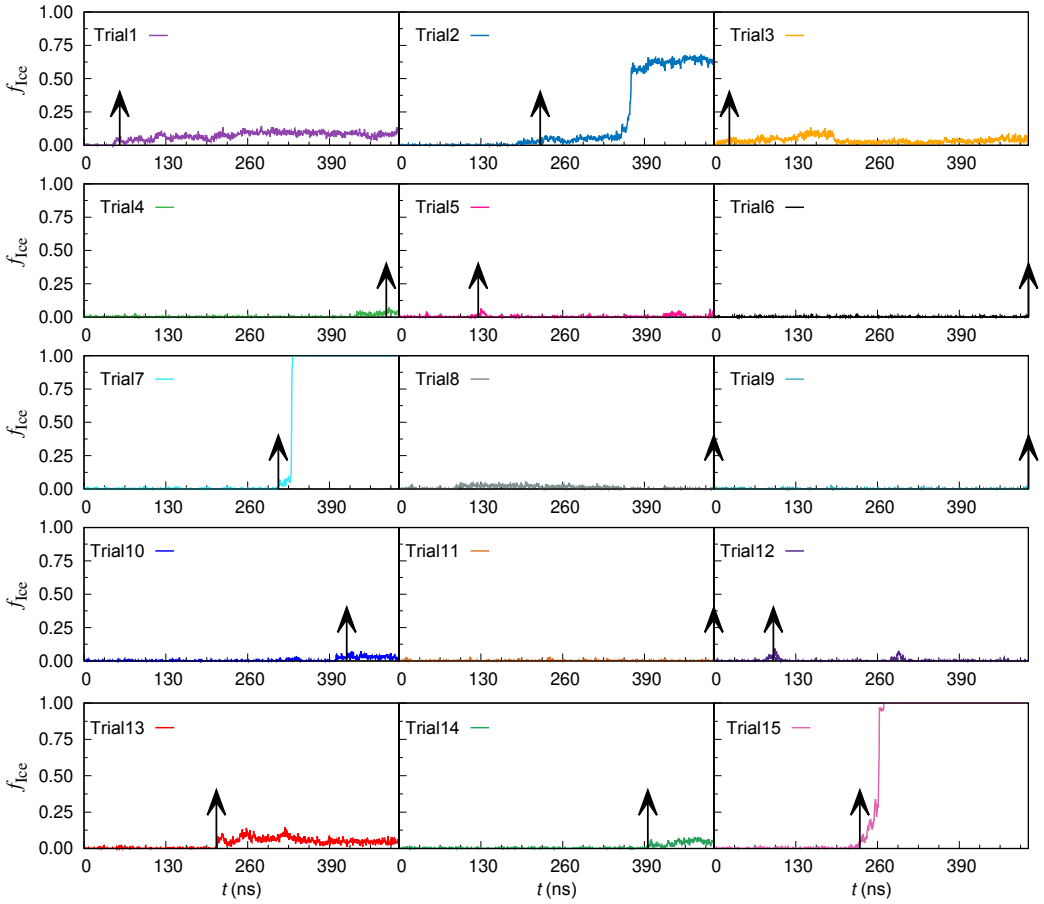

Figure 12. Fractions of cubic and hexagonal ice as a function of simulations time for 15 individual trial simulations at 300 MPa and 142 K. The point of crystallization using a 6% cutoff is denoted with an arrow in each curve.

C. Phase diagram and anomalies of ML-BOP

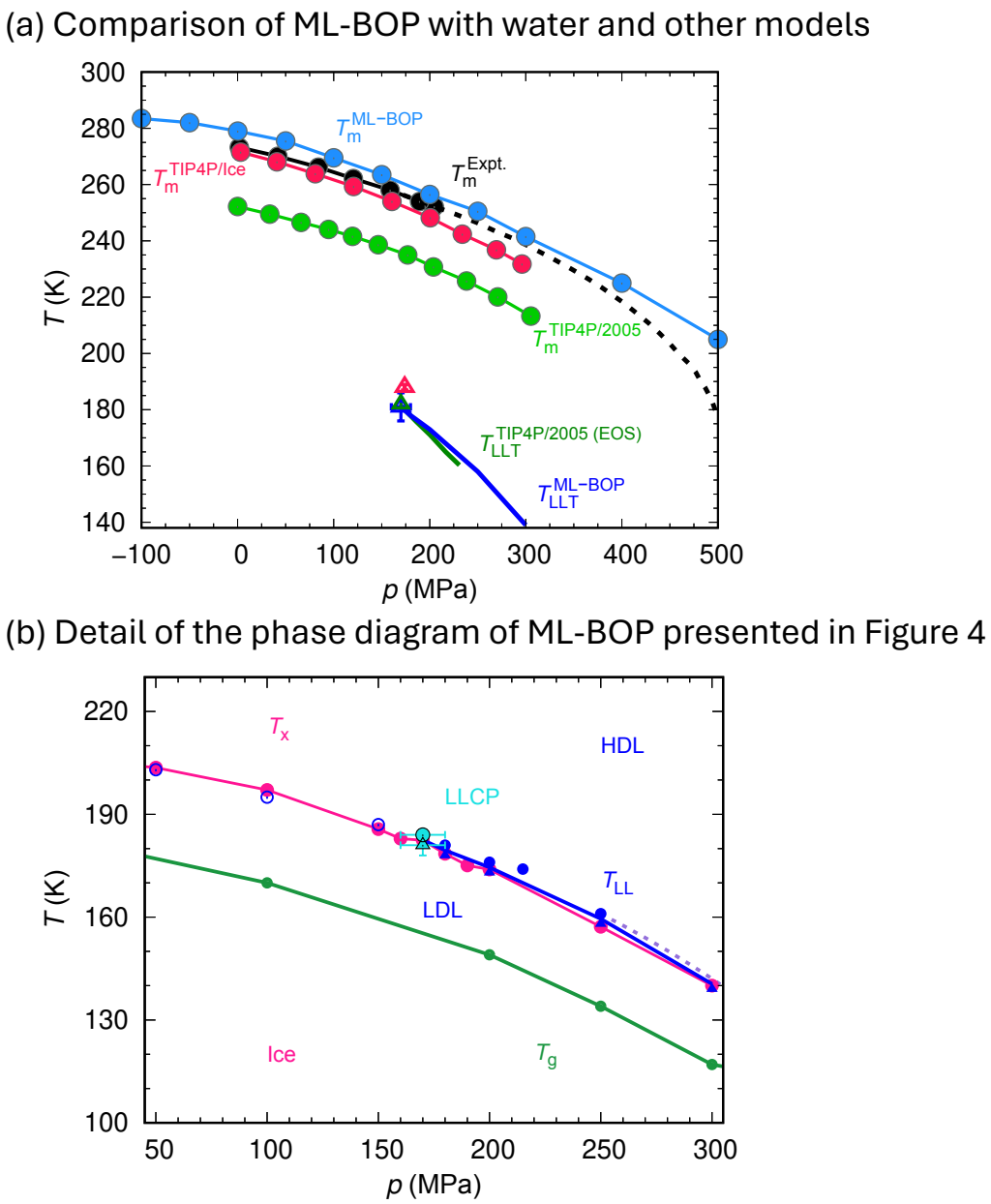

Figure S13. Phase diagram of ML-BOP. (a) Phase diagram showing the melting line T_m of water in experiments(8) (black), and water models ML-BOP(9) (blue), TIP4P/Ice (10) (red), TIP4P/2005(10) (green). The plot also shows the liquid-liquid transition line of ML-BOP (dark blue line) along with that for TIP4P/2005 computed from a two-state equation of state (TSEOS) parameterized with simulation data(11) (dark green line). The triangles show the estimated locations of LLCP for the TIP4P/2005 TSEOS(11) (dark green) and TIP4P/Ice(12) (red). (b) Detail of the phase diagram of ML-BOP presented in Figure 4, focused on the crystallization, glass transition and liquid-liquid lines in the deeply supercooled region.

Table S1. Ice Ih-liquid equilibrium melting temperatures of ML-BOP, from ref. (9)

p (MPa)	T_m (K)
-100	283.50±1
-50	282.00±1
0.1	279.00±1
50	275.50±1
100	269.50±1
150	263.50±1
200	256.50±1
250	250.50±1
300	241.50±1
400	225.00±1
500	205.00±3

Table S2. Temperatures of liquid-liquid equilibrium obtained from free energy calculations with a small cell, temperatures of liquid-liquid equilibrium or maximum heat capacity obtained from isoenthalpic decompression simulations with 216000 molecules (except for 250 MPa, which is with 8000 molecules), and temperature of maximum crystallization rate Tx obtained from isobaric cooling simulations at the fastest cooling rate that produces at least ~10% ice (Table S3). The critical pressure is 170 ± 10 MPa.

p (MPa)	T_{LL}(K) from free energy calculations	T_{LL}(K) or maximum Cp from temperature plateau of *NpH* simulations	T_x (K) *(Table S3)*
0.1	N/A	< 215 K[(a)]	207±1.0
50	N/A	203 ±1	204±1.0
100	N/A	195 ±1	197±1.0
150	N/A	187 ±1	186±1.0
170	181 ±1	184 ±1	182±1.0 (8000 molecules) 182.4±0.5 (216000 molecules)
180	179 ±1	--	179±1.0 (8000 molecules) 180.5±0.5 (216000 molecules)
190	176 ±1	--	175±1.0
200	173 ±1	176 ±1	174±1.0 (8000 molecules) 174.4±0.5 (216000 molecules)
215	--	171 ±1	
250	158 ±1	161 ±1	157±1.0
300	139 ±1	--	140±0.5 (yields 6% ice at 0.05 Kns^{-1})

(a) From the heat capacity at 0.1 MPa measured through equilibrium calculations, see Figure S14b.

Calculation of the temperature dependence of the isothermal compressibility and constant pressure heat capacity of ML-BOP at 0.1 MPa: Both isothermal compressibility and heat capacity of the ML-BOP model at 0.1 MPa are calculated from long equilibrium simulations at temperatures ranging from 215 to 378 K. The method and simulation details to calculate the compressibility as a function of temperature at 0.1 MPa are described in Supporting Information Section A. The constant pressure heat capacity as a function of temperature at 0.1 MPa is calculated from the fluctuations in enthalpy (H) as

$$C_p = \frac{1}{k_B T^2}(\langle H^2\rangle - \langle H\rangle^2),$$

where, T is the simulation temperature and k_B is the Boltzmann constant. The same simulations employed for κ_T calculations are used to compute C_p with enthalpy data being recorded every 5 ps. The entire simulation length is divided into 5 blocks to estimate the standard error. The mean of these blocks, along with the corresponding error bars are plotted in Figure S14.

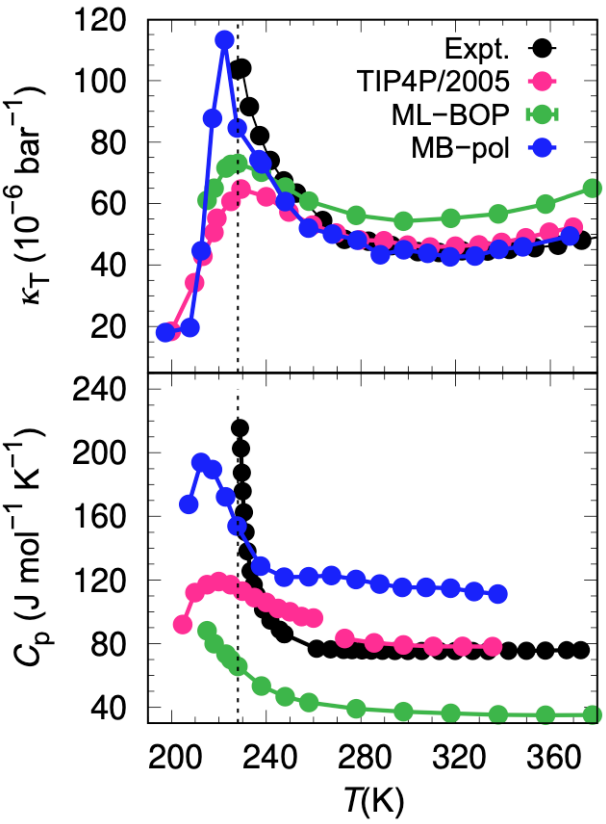

Figure S14. Temperature dependence of the isothermal compressibility κ_T (top panel) and heat capacity C_p (bottom panel) at 0.1 MPa ML-BOP, TIP4P/2005, MB-Pol and water. κ_T and C_p data of MB-Pol model are taken from ref.(13), κ_T and C_p data of TIP4P/2005 model are taken from refs. (14, 15) and ref (16), respectively. Experimental κ_T and C_p data of water are taken from refs (17-22). The maximum compressibility of ML-BOP (dashed line in both the panels) is lower than that of the experiment (well reproduced by MB-POL) and comparable in magnitude to the one of TIP4P/2005. We conjecture that the lower κ_T of ML-BOP and TIP4P/2005 reflects a positive shift of their critical pressure compared to the one in water. The temperature of maximum κ_T of ML-BOP occurs ~227 K, close to the 229 K of water. The heat capacity maximum of ML-BOP is still increasing at 215 K, the lower temperature for which the simulations could be equilibrated for 500 ns without interference of crystallization. The magnitude of the heat capacity of ML-BOP is lower than in water because the monatomic model does not have the rotational contributions. A maximum in heat capacity below the one in isothermal compressibility is consistent with the results for TIP4P-2005 and MB-POL, but not for water, for which both have been reported to coincide. The difference could reflect a lower critical pressure for water than the water models, or stem from the approximations in thermophysical properties required to determine these properties in the deeply supercooled region. Interestingly, the maximum in heat capacity of TIP4P/2005 and MB-Pol seems to coincide with the 216±1 K temperature of maximum nucleation rate determined in experiments for films.(23, 24)

D. Evolution of properties upon isoenthalpic decompression of HDL to a pressure at which is unstable.

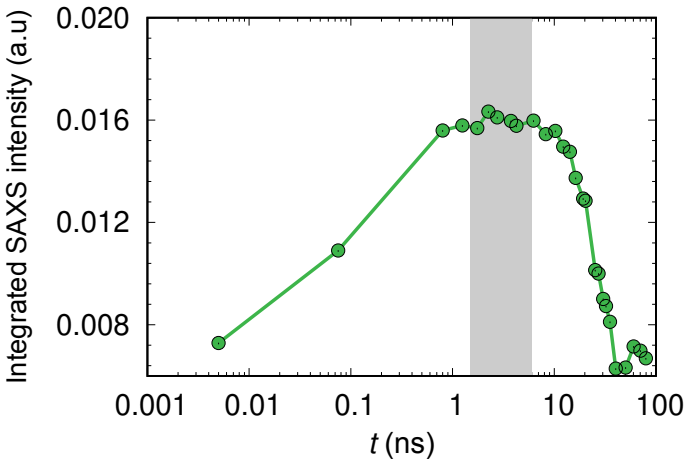

Figure S15. Integrated small angle intensity from 0.1 to 0.3 Å^{-1} along simulations of isoenthalpic decompression of HDL equilibrated at 400 MPa and 160 K to 215 MPa, using a simulation cell with 216000 molecules. The gray shade is at the center of the region of HDL and LDL coexistence (same as in Figure 5b and d). Crystallization reaches 2.5% at ~13 ns and increases steeply after 20 ns (Figures 5b and S15). The stages of the low q response are the same as in the experiments, as seen in comparison with figure 4b of Kim et al.(25))

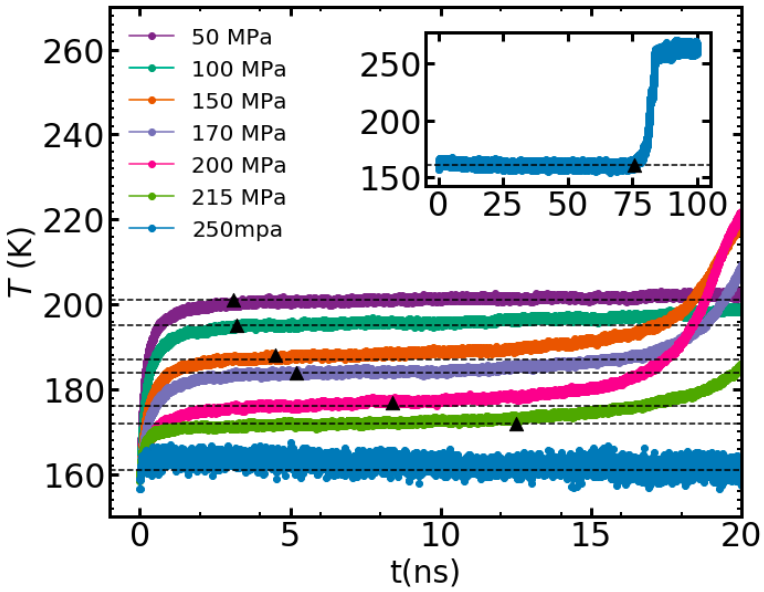

Figure S16. Temperature vs time evolution along simulations of isoenthalpic decompression of HDA to a pressure *p*. HDA is equilibrated at 255 MPa and 160 K for *p* = 50, 100, 150, 170 and 200 MPa, at 400 MPa and 160 K for *p* = 215 MPa, and at 400 MPa and 140 K for *p* = 250 MPa. We note that the enthalpy of HDA at 160 K and 400 MPa is only 3% larger/smaller than at 160 K and 255 MPa. The simulations are performed with simulation cells containing 216000 molecules, except for 250 MPa, for which the cell has 8000 molecules. The black triangles indicate the time at which 2.5% of the molecules are identified as ice (cubic and hexagonal) in the cell. The temperature of the simulation at 50 MPa increases just above 20 ns. The largest ice crystallite at 2.5% contains about 900 molecules for the simulation of decompression from 400 MPa to 215 MPa, and about 200 molecules for the decompression from 255 MPa to the other pressures.

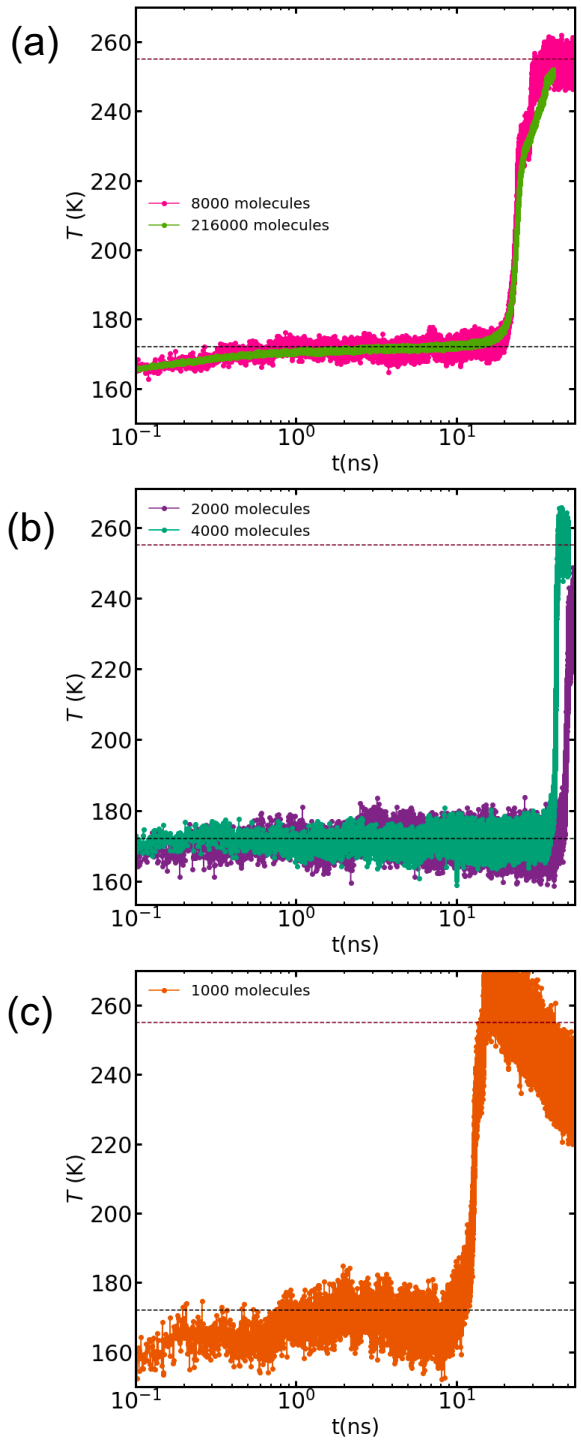

Figure S17. Temperature vs time evolution along simulations of isoenthalpic decompression of HDL equilibrated at 400 MPa and 160 K to 215 MPa using simulation cells with a) 216000 (green) and 8000 (magenta) molecules, b) 4000 (green) and 2000 (purple) molecules, and c) 1000 molecules. The upper and lower dashed lines indicate the melting temperature 255 K and liquid-liquid temperature 171 K of ML-BOP at 215 MPa. The crystallization times are comparable for all cell sizes, because the crystallites form everywhere within the cell, as a result of a low nucleation barrier.

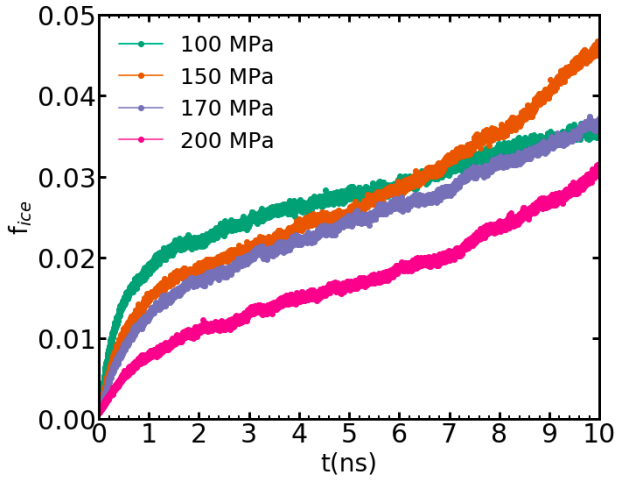

Figure S18. Fraction of ice vs time evolution along simulations of isoenthalpic decompression of HDL equilibrated at 255 MPa and 160 K to the indicated pressures, using simulation cells with 216000 molecules. 100 and 150 MPa are supercritical, 170 MPa is the critical pressure, and 200 MPa is in the two-phase liquid-liquid region.

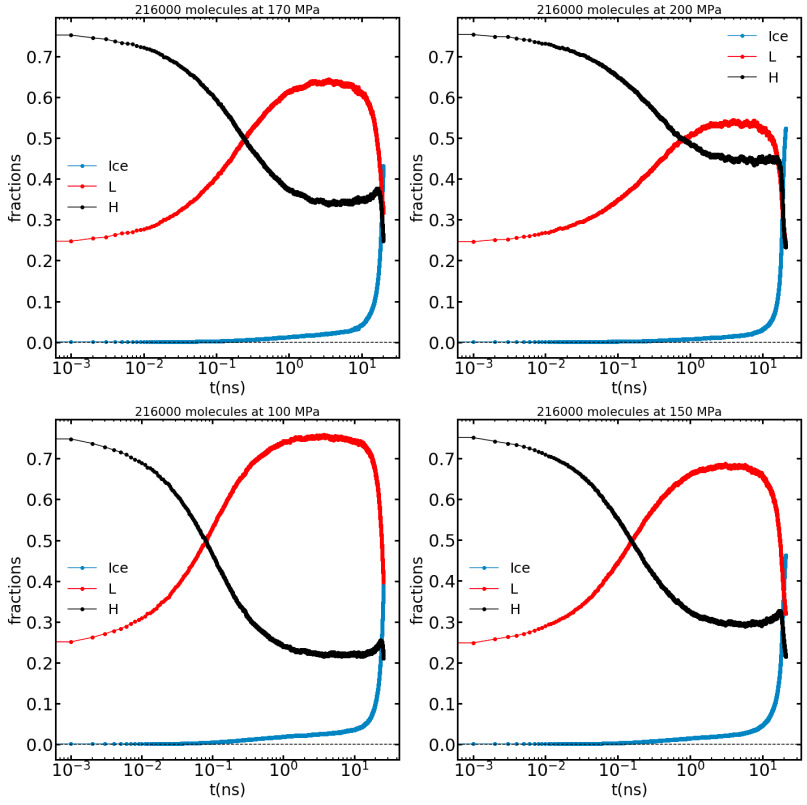

Figure S19. Evolution of the fraction of H, L, and ice along isoenthalpic decompression simulations from 255 MPa and 160 K to the critical pressure, 170 MPa, a pressure in the two-liquid region (200 MPa) and two pressures in the supercritical region (150 and 100 MPa). The qualitative response is the same in all regions. The ratio of H to L decrease as the distance from 160 K to the TLL or its supercritical continuation increase. These ratios can be modulated by the initial enthalpy of the HDL (controlled by its initial temperature and pressure). The simulations are performed with simulation cells containing 216000 molecules.

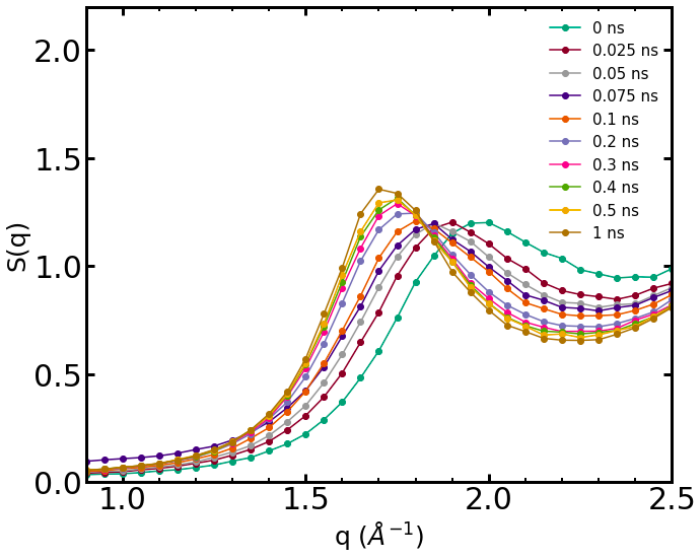

Figure S20. Initial evolution of the structure factor upon isoenthalpic decompression of HDL from 255 MPa at 160 K to 100 MPa, in the supercritical one-liquid region. Supporting Movie 2 presents the evolution of S(q) for the decompression to 215 MPa.

E. Fastest cooling rates that lead to at least 10% crystallization, and corresponding crystallization temperatures $T_x(p)$

Table S3. Temperatures of maximum crystallization rate $T_x(p)$ of ML-BOP, determined as the average over 5 independent runs of the temperature of ice nucleation at the fastest cooling rate that produces at least 10% ice in cooling simulations with 8000 or 216000 molecules.

N_{water}	p (MPa)	q_c (Kns^{-1})	T_x(K)					
			Average	T1	T2	T3	T4	T5
8000	0.1[(a)]	0.2[(a)]	207±1.0	208±0.5	207.5±0.5	206.5±0.5	206±0.5	207.5±0.5
8000	50	0.2	204±1.0	203.5±0.5	203±0.5	204.5±0.5	204±0.5	203±0.5
8000	100	0.2	197±1.0	197.5±0.5	197±0.5	196.5±0.5	197±0.5	197.5±0.5
8000	150	0.2	186±1.0	186.5±0.5	184.5±0.5	185.5±0.5	186.5±0.5	185.5±0.5
8000	160	0.2	183±1.0	183.5±0.5	183±0.5	182.5±0.5	182.5±0.5	183±0.5
8000	170	0.2	182±1.0	182±0.5	182.5±0.5	183±0.5	182±0.5	182.5±0.5
216000	170	0.2	182±0.5	182±0.5	--	--	--	--
8000	180	0.2	179±1.0	178.5±0.5	179±0.5	178.5±0.5	178±0.5	178.5±0.5
216000	180	0.5	180.5±0.5	180.5±0.5				
8000	190	0.2	175±1.0	175.5±0.5	175±0.5	175.5±0.5	174.5±0.5	175±0.5
8000	200	0.2	174±1.0	174±0.5	174.5±0.5	174.5±0.5	173.5±0.5	173±0.5
216000	200	0.2	174.4±0.5	174.4±0.5	--	--	--	--
8000	250	0.1	157±1.0	156.5±0.5	159.5±0.5	156±0.5	156.5±0.5	157.5±0.5
8000	300	<0.05	140±0.5[(b)]	140±0.5	--	--	--	--

(a) From ref. (9);(b) at q = 0.05 Kns^{-1}, which results in 6% ice

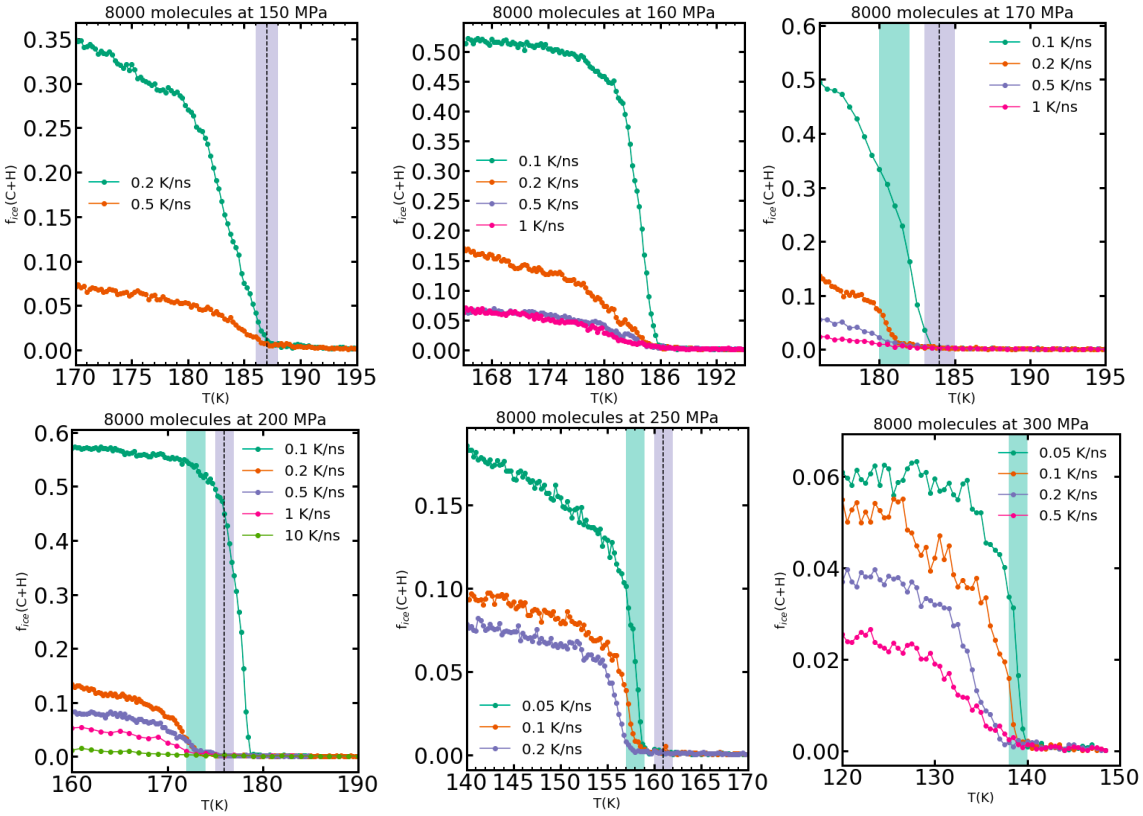

Figure S21. Fraction of ice (cubic and hexagonal) as a function of temperature along cooling simulations with 8000 ML-BOP water molecules at various cooling rates. The cyan vertical band indicates $T_{LL}(p)$ computed from the free energy calculations with the 192 molecules cell, and the darker blue band the $T_{LL}(p)$ or Widom line of maximum heat capacity $C_p^{max}(p)$ computed from the plateau of the temperature in the isoenthalpic simulations of decompression of HDL to the corresponding pressure. Fig. S2 of ref. (9) presents the fraction of ice as a function of temperature in cooling simulations of 8000 molecule cells of ML-BOP at 0.1 MPa for cooling rates 0.05 to 10 Kns^{-1}.

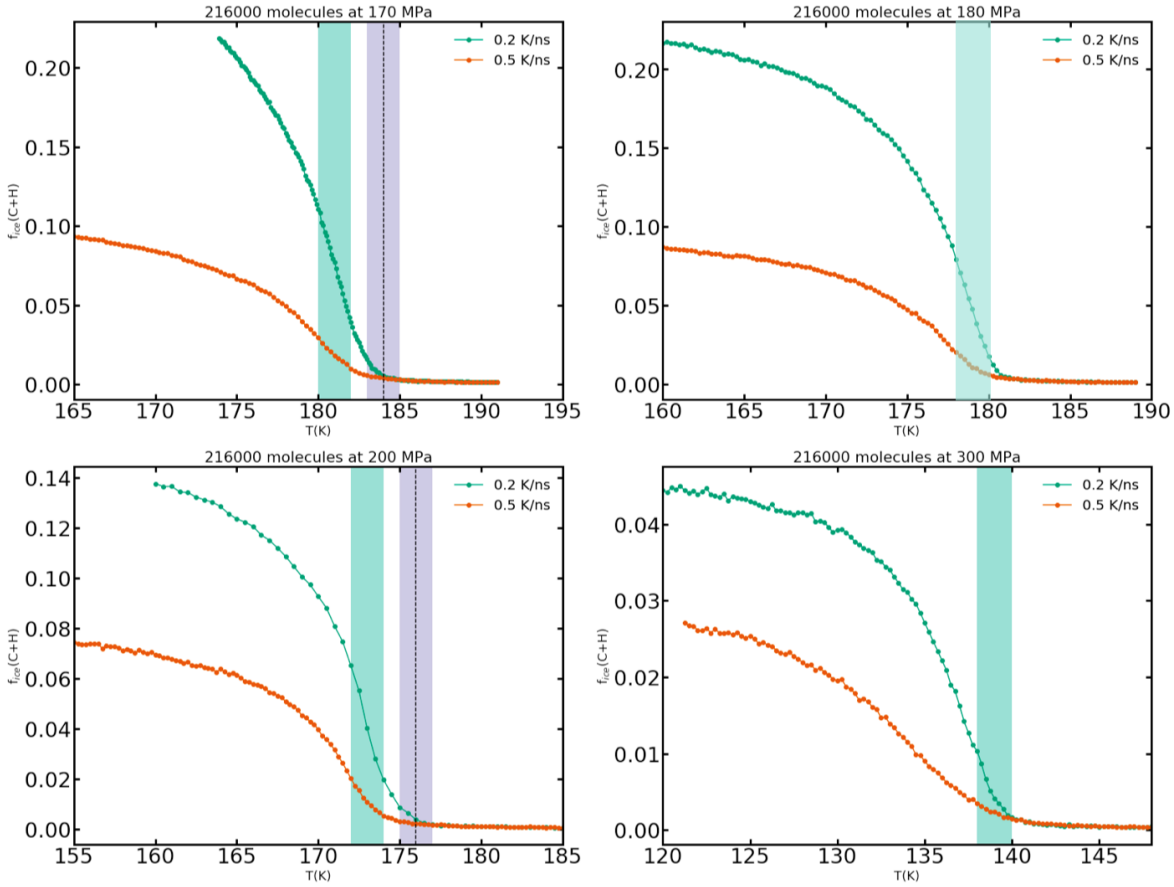

Figure S22. Fraction of ice (cubic and hexagonal) as a function of temperature along cooling simulations with 216000 ML-BOP water molecules at various cooling rates. The greenish cyan vertical band indicates $T_{LL}(p)$ computed from the free energy calculations with the 192 molecules system, and the darker purplish blue line the $T_{LL}(p)$ or Widom line of maximum heat capacity $C_p^{max}(p)$ computed from the plateau of the temperature from isoenthalpic simulations of decompression of HDL to the corresponding pressure.

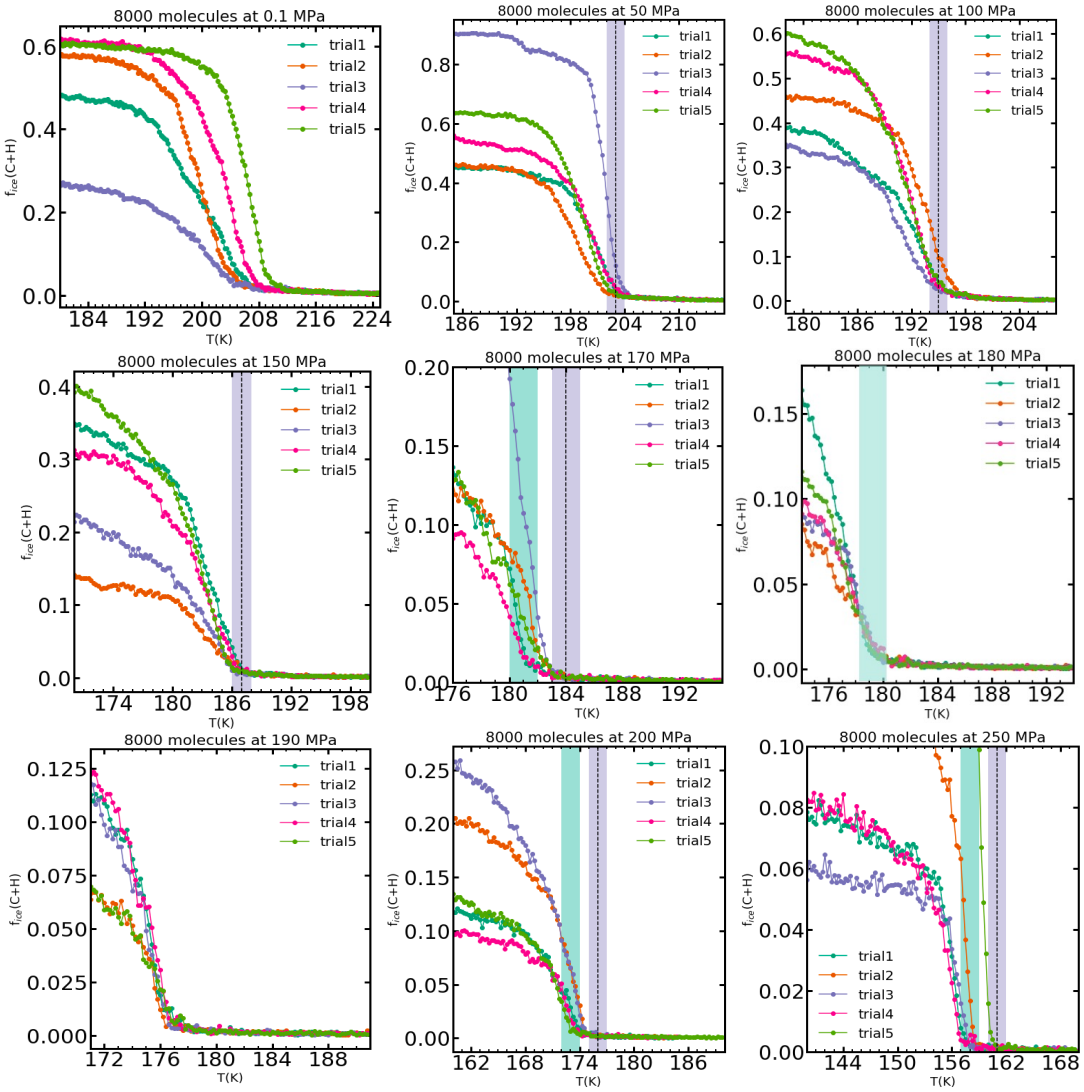

Figure S23. Fraction of ice (cubic and hexagonal) as a function of temperature along 5 independent cooling simulations at $q_c(p)$ with 8000 ML-BOP water molecules. The greenish cyan band indicates the $T_{LL}(p)$ from free energy calculations with the 192 molecules cell, and the purplish blue line the $T_{LL}(p)$ or temperature of maximum heat capacity obtained from the plateau of the isoenthalpic decompression simulations with 216000 molecules.

F. Glass transition temperature of ML-BOP as a function of pressure, intersection with the liquid-liquid transformation temperature, and impact on the density of hyperquenched glasses

The gray line in Figure 4 shows the non-equilibrium HDL to LDL transformation temperatures $T_S(p)$, computed as the locus of maximum $S(0)$ along the cooling simulations (Figure 1). $T_S(p)$ is an effective limit of stability of HDL, although it needs not coincide with the thermodynamic spinodal because it is measured out of equilibrium at a high cooling tate. $T_S(p)$ of ML-BOP cooled at 10 K ns^{-1} starts at the LLCP and crosses the glass transition line at 300 MPa (Figures 4), truncating the HDL to LDL transformation and freezing in the largest long-range correlations at pressures 250 to 300 MPa, well above p_c of the model. We interpret that the crossover at higher pressures originates in the lower fragility of diffusion in ML-BOP compared to water(26) and TIP4P/2005(27) We interpret that the crossover at higher pressures originates in the shallower temperature dependence (and apparently also lower fragility) of the diffusion coefficient in ML-BOP compared to water(26) and TIP4P/2005(27) (see discussion in Supp. Section F). We anticipate that the interplay between glass transition and liquid-liquid transformation in water resembles the one of TIP4P/2005, and not the one of ML-BOP. As the maximum $S(0)$ in the glass at 77 K and ~250 MPa is lower than for the liquid crossing the LLCP (Figure 1), the location of the critical pressure could be disambiguated by measuring $S(0)$ of glasses prepared at a wide range of cooling rates that modulate where the glass transition crosses the LLT and Widom line, to find the absolute maximum of long-range correlations in the glasses.

Figure S24 presents the $T_g(p)$ of ML-BOP calculated as the temperature at which the molecules displace less than 0.8 Å over 100 ps in 10 K ns^{-1} isobaric cooling simulations. $T_g(p)$ of ML-BOP is lower than for TIP4P/2005 at the same cooling rate(4) (Figure S24b), cutting the LLT line of the model at 110 K and 360 MPa (Figure S24a and green triangle in Figure S24b). The slope of $T_g(p)$ of ML-BOP is negative in the region of LDA and turns to positive in the region of HDA (Figure S24), same as reported for all-atom models of water and experiments,(28, 29). Indeed, the slopes of T_g vs pressure are very similar for each liquid phase in the two models. Within the perspective of excess entropy scaling of the viscosity and diffusion coefficients,(30) the agreement in the slopes between the slopes of $T_g(p)$ in the two models may be interpreted as arising from the similarity of the equations of state of both models and $\mathrm{d}S/\mathrm{d}p)_T = -\mathrm{d}V/\mathrm{d}T)_p$.

Nevertheless, the magnitude of T_g for the HDL of ML-BOP cooled at 10 Kns^{-1} is about 70 K lower than for TIP4P/2005 cooled at the same rate (Figure S24). This indicates much higher mobility in ML-BOP's supercooled HDL compared to TIP4P/2005. We interpret that the crossover at higher pressures originates in the lower fragility of diffusion in ML-BOP compared to water**(26)** and TIP4P/2005**(27)**. The lower fragility of HDL in ML-BOP is akin to that of the monatomic water model mW,**(31)** suggesting that in both cases it originates in the smoother free energy landscape experienced in the diffusion of the coarse-grained models. The relative closeness (about 20 K) of the glass transition of LDL in ML-BOP and TIP4P/2005 (Figure S24, pressures below the corresponding white filled triangles) suggest that the discrepancy is

less pronounced when the liquid has Arrhenius diffusion (strong liquid) as expected for the tetrahedrally coordinated LDL. We consider the results of TIP4P/2005 of Gartner et al. in ref (4) more likely for water.

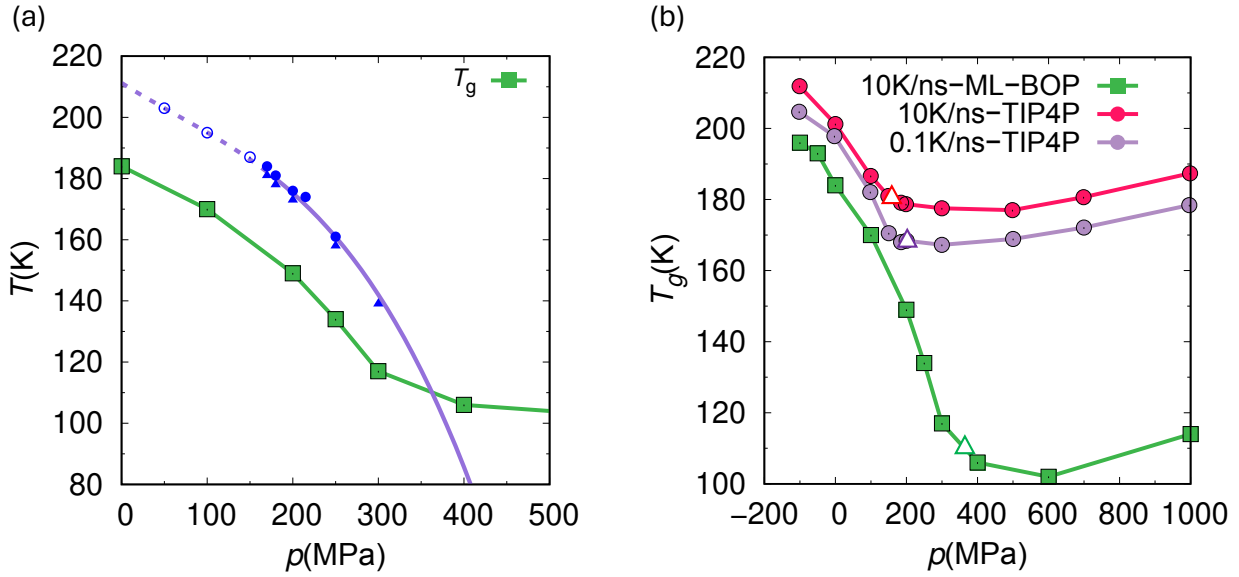

Figure S24. Glass transition temperature $T_g(p)$ of ML-BOP obtained from isobaric cooling simulations at 10 Kns^{-1} from with 8000 molecules at pressures p from -100 to 1000 MPa (green squares). (a) Filled blue symbols represent points along the LLT (triangles obtained from free energy calculations, circles from isoenthalpic decompression of HDL), the open blue circles are the loci of maximum heat capacity in the supercritical region (obtained from the plateau of the temperature of isoenthalpic decompression). The purple line is a 3rd order polynomial fit of the LLT (solid line) and its supercritical continuation (dashed line). The glass transition temperature obtained from 10 Kns^{-1} cooling simulations crosses the LLT at an extrapolated 360 K MPa. (b) $T_g(p)$ of ML-BOP measured at 10 Kns^{-1} (green squares), $T_g(p)$ of TIP4P/2005 determines from cooling simulations with rates 10 (red circles) and 0.1 Kns^{-1} (purple circles) from Gartner et al. ref. (4). The minimum in $T_g(p)$ for each curve occurs at pressures just above the crossing of $T_g(p)$ with $T_{LL}(p)$ of the model at the corresponding cooling rate. For ML-BOP, the crossing of $T_{LL}(p)$ and $T_g(p)$ cooled at 10 Kns^{-1} occurs at an extrapolated 360 MPa and 110 K Z(white filled green triangle, see also Figure 4), while for TIP4P/2005 the crossing between $T_g(p)$ and the locus of maximum long-range correlations S(0) at that cooling rate(4) occurs at 150 MPa and 181 K at 10 Kns^{-1} (white filled red triangle) and at 185 MPa and 168 K at 0.1 Kns^{-1} (white filled purple triangle).

The HDL to LDL transition can be completed by ML-BOP prior to vitrification in cooling simulations at pressures between p_c = 170±10 MPa and ~360 MPa, for which $T_g(p) < T_{LL}(p)$. However, the liquid-liquid transformation occurs below the equilibrium $T_{LL}(p)$ at the high cooling rates required to bypass crystallization. The locus of the non-equilibrium transformation can be gleaned from the temperatures $T_S(p)$ of maximum $S(0)$ along the cooling simulations (Figure 1). $T_S(p)$ is an effective limit of stability of HDL, although it needs not coincide with the thermodynamic spinodal. $T_S(p)$ of ML-BOP cooled at 10 K ns^{-1} starts at the LLCP and crosses the glass transition line at 300 MPa (Figure 4), truncating the HDL to LDL transformation and freezing in the largest long-range correlations at pressures 250 to 300 MPa, well above p_c = 170±10 MPa of the model (Figure 1).

The density of the glasses obtained by isobaric hyperquenching of ML-BOP display a sigmoidal shape with maximum slope between 250 and 300 MPa (Figure S24).**(32)** These are the pressures at which ML-BOP glasses present the largest long-range density correlations (Figure 1), because they vitrify as they transition from HDL to LDL. Hyperquenched glasses obtained at 250 to 300 MPa are in the density range of the recently uncovered medium density amorphous ice (MDA) made by ball-milling ice at 77 K and recovered at 0.1 MPa**(33)** (Figure S24). However, the HQG with density intermediate between those of LDA and HDA have significant long-range structural correlations (Figure 1), while there are no strong signatures in the low q region of $S(q)$ of MDA (if there are, they are hidden under strong Porod-law dispersion).**(33)** It has not yet been established whether the shearing involved in ball-milling enables the sampling of

distinct states not visited during hyperquenching protocols, or there are equivalencies in the structure and thermodynamics of ball-milled and hyperquenched water glasses.

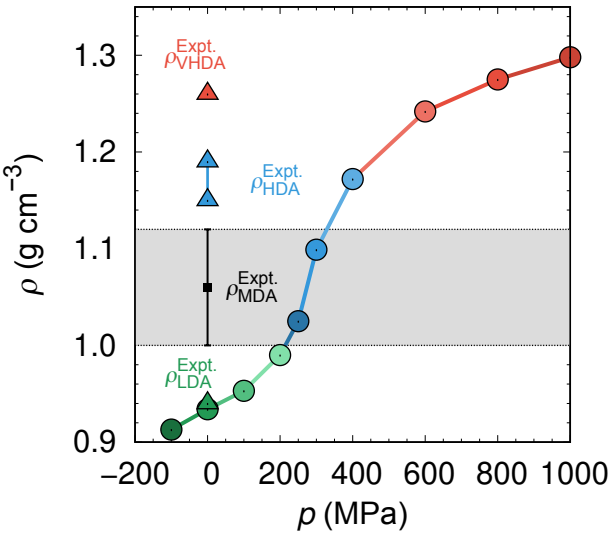

Figure S25. Density of various water glasses. Circles show the density of hyperquenched glasses produced by isobaric cooling of ML-BOP at 10 K ns^{-1} to 78 K, determined in ref (32). Triangles show the experimental densities at 0.1 MPa of LDA (green),(34, 35) HDA (blue),(36-40) and VHDA (red),(40). The density of these glasses is accurately reproduced by the ML-BOP model.(32) The experimental density of MDA and its error bar are shown in black.(33) The density of the HQG prepared at 250 and 300 MPa falls with the 1.06 ± 0.06 g cm^{-3} density range of MDA (gray band) prepared by ball-milling ice at 77 K subject to unknown pressure and shear rate before recovering the sample at 0.1 MPa.(33)

G. Simulation conditions for calculation of the LLT

Table S4. Range of temperatures at which we perform simulations with periodic simulation cells containing 192 water molecules to calculate the relative free energies of the liquids.

p (MPa)	T (K)
300	135, 136, 136.5, 137, 137.5, 139, 140, 142
250	156, 157, 158, 159, 160
200	170, 173, 174, 175, 176, 178, 183
180	177, 178, 179, 180, 184
170	179, 180, 181, 182,183
160	183, 184, 185, 186, 188,190
50	198, 200, 202,203, 204, 206, 207, 208, 212

Table S5. Number of molecules N, decompression pressure p, and HDL equilibration pressure p_{HDL} and temperature T_{HDL} of the NpH simulations of decompression of HDL.

N	P(MPa)	p_{HDL}(MPa)	T_{HDL}(K)
8000	250	255	140
216000	215	400	160
8000	215	400	160
216000	200	255	160
216000	170	255	160
216000	150	255	160
216000	100	255	160
216000	50	255	160

H. Movie Captions

Movie 1. Evolution of a simulation cell with 216000 water molecules along an isobaric isoenthalpic (NpH) simulation that instantaneously decompresses HDL from 160 K and 400 MPa to 215 MPa. Ice is shown with cyan sticks, 4-coordinated molecules L with blue sticks, and higher-coordination molecules with red sticks. The movie shows the evolution over the first 21 ns, with configurations every 20 ps.

Movie 2. Evolution of the structure factor S(q) for a system of 216000 water molecules along an isobaric isoenthalpic (NpH)decompression simulation from 160 K and 400 MPa to 215 MPa. The dotted lines in pink and green indicate the reference peaks in $S(q)$ for HDL and LDL, respectively. The pink region denotes the S(q) corresponding to our initial HDL configuration of the simulation and blue region presents its evolution along the simulation.

Movie 3. Evolution of a simulation cell with 216000 water molecules along an isobaric isoenthalpic (NpH) simulation that instantaneously decompresses HDL from 160 K and 255 MPa to 170 MPa. Ice is shown with cyan sticks, 4-coordinated molecules L with blue sticks, and higher-coordination molecules with red sticks. The movie shows the evolution over the first 21 ns, with configurations every 20 ps.

Movie 4. Formation of ice (cyan) in a system of 216000 water molecules along isoenthalpic decompression simulations from 255 MPa, 160 K to 170 MPa for 21 ns. Each frame of the movie represents 10 ps of the simulation trajectory. Ice comprises cubic and hexagonal ice identified with CHILL+.**(41)**

I. Input files that generate the simulation trajectories.

Decompression of the file input-files.zip results in a directory that contains three folders that contain LAMMPS input files to generate simulations used to compute the free energies (directory **NPT-170mpa-192molecules**), the NPH simulations of decompression of HDL (directory **NPH-170mpa-216000 molecules**), and the cooling simulations used to compute the crystallization temperatures (directory **Tx-170MPa-8000molecules**).

SUPPORTING REFERENCES

1. F. Sedlmeier, D. Horinek, R. R. Netz, Spatial Correlations of Density and Structural Fluctuations in Liquid Water: A Comparative Simulation Study. *Journal of the American Chemical Society* **133**, 1391-1398 (2011).
2. D. Dhabal, K. T. Wikfeldt, L. B. Skinner, C. Chakravarty, H. K. Kashyap, Probing the triplet correlation function in liquid water by experiments and molecular simulations. *Physical Chemistry Chemical Physics* **19**, 3265-3278 (2017).
3. L. B. Skinner, C. J. Benmore, B. Shyam, J. K. R. Weber, J. B. Parise, Structure of the floating water bridge and water in an electric field. *Proceedings of the National Academy of Sciences* **109**, 16463-16468 (2012).
4. T. E. Gartner, S. Torquato, R. Car, P. G. Debenedetti, Manifestations of metastable criticality in the long-range structure of model water glasses. *Nature Communications* **12**, 3398 (2021).

5. Anonymous, Jean-Pierre Hansen, I.R. McDonald - Theory of Simple Liquids, Third Edition (2006, Academic Press).
6. M. D. Allen, D. J. Tildesley, *Computer Simulation of Liquids* (Oxford University Press, New York, 1989).
7. W. Humphrey, A. Dalke, K. Schulten, VMD: Visual molecular dynamics. *Journal of Molecular Graphics* **14**, 33-38 (1996).
8. H. Kanno, R. J. Speedy, C. A. Angell, Supercooling of Water to -92°C Under Pressure. *Science* **189**, 880-881 (1975).
9. D. Dhabal, S. K. R. S. Sankaranarayanan, V. Molinero, Stability and Metastability of Liquid Water in a Machine-Learned Coarse-Grained Model with Short-Range Interactions. *The Journal of Physical Chemistry B* **126**, 9881-9892 (2022).
10. J. L. F. Abascal, E. Sanz, R. G. Fernández, C. Vega, A potential model for the study of ices and amorphous water: TIP4P/Ice. *J. Chem. Phys.* **122**, 234511 (2005).
11. R. S. Singh, J. W. Biddle, P. G. Debenedetti, M. A. Anisimov, Two-state thermodynamics and the possibility of a liquid-liquid phase transition in supercooled TIP4P/2005 water. *J. Chem. Phys.* **144**, 144504 (2016).
12. P. G. Debenedetti, F. Sciortino, G. H. Zerze, Second critical point in two realistic models of water. *Science* **369**, 289-292 (2020).
13. T. E. Gartner III *et al.*, Anomalies and local structure of liquid water from boiling to the supercooled regime as predicted by the many-body MB-pol model. *The Journal of Physical Chemistry Letters* **13**, 3652-3658 (2022).
14. F. Martelli, Unravelling the contribution of local structures to the anomalies of water: The synergistic action of several factors. *The Journal of chemical physics* **150**, 094506 (2019).
15. J. L. F. Abascal, C. Vega, A general purpose model for the condensed phases of water: TIP4P/2005. *The Journal of Chemical Physics* **123**, 234505 (2005).
16. H. Pathak *et al.*, The structural validity of various thermodynamical models of supercooled water. *The Journal of chemical physics* **145** (2016).
17. K. H. Kim *et al.*, Maxima in the thermodynamic response and correlation functions of deeply supercooled water. *Science* **358**, 1589-1593 (2017).
18. G. S. Kell, Isothermal compressibility of liquid water at 1 atm. *Journal of Chemical and Engineering Data* **15**, 119-122 (1970).
19. C. Angell, W. Sichina, M. Oguni, Heat capacity of water at extremes of supercooling and superheating. *The Journal of Physical Chemistry* **86**, 998-1002 (1982).
20. H. Pathak *et al.*, Enhancement and maximum in the isobaric specific-heat capacity measurements of deeply supercooled water using ultrafast calorimetry. *Proceedings of the National Academy of Sciences* **118**, e2018379118 (2021).
21. W. Wagner, A. Pruß, The IAPWS formulation 1995 for the thermodynamic properties of ordinary water substance for general and scientific use. *Journal of physical and chemical reference data* **31**, 387-535 (2002).
22. R. Speedy, C. Angell, Isothermal compressibility of supercooled water and evidence for a thermodynamic singularity at− 45 C. *The Journal of Chemical Physics* **65**, 851-858 (1976).
23. G. A. Kimmel *et al.*, Homogeneous ice nucleation rates and crystallization kinetics in transiently-heated, supercooled water films from 188 K to 230 K. *The Journal of Chemical Physics* **150** (2019).
24. Y. Xu, N. G. Petrik, R. S. Smith, B. D. Kay, G. A. Kimmel, Growth rate of crystalline ice and the diffusivity of supercooled water from 126 to 262 K. *Proceedings of the National Academy of Sciences* **113**, 14921-14925 (2016).
25. K. H. Kim *et al.*, Experimental observation of the liquid-liquid transition in bulk supercooled water under pressure. *Science* **370**, 978-982 (2020).
26. H. Chan *et al.*, Machine learning coarse grained models for water. *Nature Communications* **10**, 379 (2019).
27. D. Rozmanov, P. G. Kusalik, Transport coefficients of the TIP4P-2005 water model. *The Journal of Chemical Physics* **136**, 044507 (2012).
28. P. Gallo *et al.*, Water: A Tale of Two Liquids. *Chemical Reviews* **116**, 7463-7500 (2016).
29. N. Giovambattista, T. Loerting, B. R. Lukanov, F. W. Starr, Interplay of the Glass Transition and the Liquid-Liquid Phase Transition in Water. *Scientific Reports* **2**, 390 (2012).
30. J. C. Dyre, Perspective: Excess-entropy scaling. *The Journal of chemical physics* **149** (2018).
31. V. Molinero, E. B. Moore, Water Modeled As an Intermediate Element between Carbon and Silicon. *The Journal of Physical Chemistry B* **113**, 4008-4016 (2009).
32. D. Dhabal, V. Molinero, Kinetics and Mechanisms of Pressure-induced Ice Amorphization and Polyamorphic Transitions in a Machine-learned Coarse-Grained Water Model. 10.26434/chemrxiv-2023-llft6 (2023).

33. A. Rosu-Finsen *et al.*, Medium-density amorphous ice. *Science* **379**, 474-478 (2023).
34. T. Loerting, C. Salzmann, I. Kohl, E. Mayer, A. Hallbrucker, A second distinct structural " state " of high-density amorphous ice at 77 K and 1 bar. *Physical Chemistry Chemical Physics* **3**, 5355-5357 (2001).
35. K. Winkel, D. T. Bowron, T. Loerting, E. Mayer, J. L. Finney, Relaxation effects in low density amorphous ice: Two distinct structural states observed by neutron diffraction. *The Journal of Chemical Physics* **130**, 204502 (2009).
36. D. Mariedahl *et al.*, X-ray Scattering and O–O Pair-Distribution Functions of Amorphous Ices. *The Journal of Physical Chemistry B* **122**, 7616-7624 (2018).
37. K. Amann-Winkel, D. T. Bowron, T. Loerting, Structural differences between unannealed and expanded high-density amorphous ice based on isotope substitution neutron diffraction. *Molecular Physics* **117**, 3207-3216 (2019).
38. O. Mishima, L. D. Calvert, E. Whalley, 'Melting ice' I at 77 K and 10 kbar: a new method of making amorphous solids. *Nature* **310**, 393-395 (1984).
39. O. Mishima, L. D. Calvert, E. Whalley, An apparently first-order transition between two amorphous phases of ice induced by pressure. *Nature* **314**, 76-78 (1985).
40. T. Loerting, C. G. Salzmann, K. Winkel, E. Mayer, The relation between high-density and very-high-density amorphous ice. *Physical Chemistry Chemical Physics* **8**, 2810-2818 (2006).
41. A. H. Nguyen, V. Molinero, Identification of clathrate hydrates, hexagonal ice, cubic ice, and liquid water in simulations: The CHILL+ algorithm. *The Journal of Physical Chemistry B* **119**, 9369-9376 (2015).